Heriot-Watt University

Photoracemization and excited state relaxation through non-adiabatic pathways in chromium (III) oxalate ions

Zurek, Justyna M; Paterson, Martin J

Photoracemization and excited state relaxation through non-adiabatic pathways in chromium (III) oxalate ions

Justyna M. Żurek and Martin J. Paterson

Additional information on J. Chem. Phys.
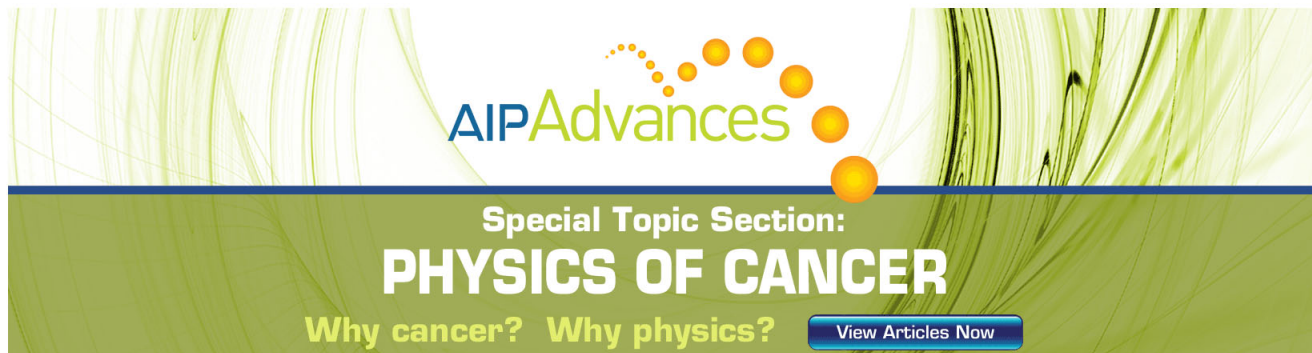
Photoracemization and excited state relaxation through non-adiabatic pathways in chromium (III) oxalate ions

Justyna M. Żurek and Martin J. Paterson[a)]
Institute of Chemical Sciences, School of Engineering and Physical Sciences, Heriot-Watt University, Edinburgh EH14 4AS, Scotland

Computational studies on the photochemistry of the open-shell chromium oxalate $[Cr(C_2O_4)_3]^{3-}$ ion, including its non-adiabatic relaxation pathways, have been performed. The presence of the peaked conical intersection of a quasi-Jahn-Teller type, connecting the ^4T state with $^4A_2$ ground state, accounts for the observed photoinduced racemization. This involves the rupture of one of the Cr–O bonds and the complex forms an unstable trigonal bipyramid form that connects both ground state stereoisomers with the excited quartet manifold. Intersystem crossing seams have been located between the ^4T and lower lying ^2E state which can quench the quartet reaction and lead to $^2E \rightarrow {}^4A_2$ emission. © *2012 American Institute of Physics*. [http://dx.doi.org/10.1063/1.4736561]

I. INTRODUCTION

The photochemistry of systems containing Cr (III) ions has been a subject of increasing investigation over recent years.[1–6] Despite the fact that the main spectroscopic features have been described for a wide range of Cr (III) complexes, the nature of reactive states and photochemical relaxation mechanisms is still not known for many of them. Often with transition metal complexes electronic transitions from the ground electronic state proceed to a manifold of many electronic states that are very close in energy. Thus, identification of the initial absorbing state and the photochemistry occurring from it can be rather challenging.

The subject of this paper are studies on the photochemical properties and photoprocesses occurring in the chromium oxalate ion $[Cr(C_2O_4)_3]^{3-}$, which is an open-shell compound sometimes described as "a molecular version of ruby" because of their similar spectroscopic properties. Due to the lack of exchange interactions, when incorporated into stoichiometric compounds, this system has proved to be a better model for studies on the energy migration processes occurring in ruby and similar systems.

Absorption of a photon often results in a chemical change to the system, which can be caused by dissociation of the absorbing molecules into reactive fragments, or by direct reaction of the electronically excited species, including, for example, photoinduced isomerisation. Alternatively, the absorbing molecule may undergo radiative loss of excitation energy (i.e., light emission - luminescence), and return to the ground state without any chemical transformation. Examples of such radiative phenomena are fluorescence and phosphorescence (radiative processes resulting in spin-state conservation or change, respectively). Chemiluminescence is another radiative process in which a ground state chemical reaction produces an excited state product, which undergoes radiative decay to the (new) product ground state species. Processes caused by the absorption of photon that take place in coordinated $[Cr(C_2O_4)_3]^{3-}$ compounds and their participation in energy migration were first described by Milos and coworkers.[7] There has been no fluorescence observed in systems with chromium oxalates at the temperatures at which phosphoresce is quenched, a feature whose explanation caused much debate in the past. Possible explanations included nonradiative depopulation of the $^4T_2$ state, or relaxation pathways through ^2E states.[8,9] Luminescence in Cr (III) oxalate systems has been found to be dependent on the temperature and concentration of $[Cr(C_2O_4)_3]^{3-}$ in these systems. Milos and co-workers reviewed the behaviour of luminescence in such systems and noted that, for example, in concentrated oxalate systems, for temperatures above 4.2 K the strength of the luminescence falls, and for the systems where Cr (III) is doped into host lattices for temperatures above 100 K, the luminescence is quenched, and the thermally induced back intersystem crossing (BISC) from the ^2E state to the $^4T_2$ state becomes important.[7] A narrow luminescence band in the spectra of $[Cr(C_2O_4)_3]^{3-}$ systems has been attributed to a $^2E \rightarrow {}^4A_2$ transition (543 nm) which is induced by efficient intersystem crossing (ISC) from $^4T_2$. It can also be quenched via thermal population of the $^4T_2$ state, due to the small energy gap between these $^4T_2$ and ^2E states. This is common for systems in oxygen environments in which the ^2E state is located below the $^4T_2$ state. The role of $^4T_2$ and ^2E states is crucial in determining the relaxation pathways and photochemistry of different Cr (III) complexes, however, a detailed theoretical study on such systems is currently lacking.

$[Cr(C_2O_4)_3]^{3-}$ is known to exist in two optical isomers. Experimental studies on the racemization reaction of this system show that its activation energy in water is 13.3 kcal mol^{-1}, and the racemization rate increases with the presence of an acid, alkali, or inert salt, and decreases in organic solvents.[10] It was first reported in 1959 that this reaction is photoinduced and further studies have focused on the mechanism of this photoprocess.[11] Spees and Adamson

_____
[a)]Author to whom correspondence should be addressed. Electronic mail: m.j.paterson@hw.ac.uk.

suggested that the detachment of one end of $(C_2O_4)^-$ from the full $[Cr(C_2O_4)_3]^{3-}$ complex and mono-aquation of the system could be induced by light. This was hypothesised on the basis of the lack of catalyst and small solvent medium effect on the quantum yield of the reaction. This detachment is a first step of the oxygen exchange reaction common for oxalate systems and the authors proposed that it could be followed by hydration of the formed monodentate intermediate, or intramolecular oxalate-oxalate displacement.[12]

To explain the mechanism of this photoracemization and other photoprocesses occurring in this system, detailed computational studies are required. Previous studies on Cr (III) complexes have turned out to be very challenging, both experimentally and computationally.[5,6] The use of high-level multiconfigurational methods in inorganic chemistry is still challenging, but recent work has shown the potential of such methods applied to problems in inorganic photochemistry involving non-adiabatic effects.[13–15] Recently, we have looked at the mechanisms of photoaquation reactions of the $[Cr(tn)_3]^{3+}$ complex, where tn is 1,3-diaminopropane. The complete active space self-consistent field (CASSCF) method in conjunction with time-dependent density functional theory (TD-DFT) was used to model features on the ground and excited state potential energy surfaces (PES). Aspects of photoproduct formation in these reactions were explained as involving low-coordination unsaturated geometries that are conical intersections (CIs).[16] Similarly, here we have computationally investigated the mechanisms for radiationless deactivation through the quartet and doublet manifolds of $[Cr(C_2O_4)_3]^{3-}$, to explain the mechanism for photoinduced racemization amongst stereoisomers. We see interesting similarities and differences between these two paradigm Cr (III) complexes. We also looked to determine the ordering and characterization of the main excited electronic states involved in the photochemistry, as such features have not been studied to date. In Sec. II., an introduction to the spectroscopy of Cr (III) complexes will be given, followed by our TD-DFT and CASSCF results on $[Cr(C_2O_4)_3]^{3-}$ in Sec. IV.

II. BACKGROUND

A. General spectroscopic properties of Cr (III) O_h systems

The ordering of the main absorbing states has a key importance for energy transfer and energy migration processes. Kane-Maguire adapted the Jablonski state energy level diagram to O_h Cr (III) complexes to describe the transitions and processes occurring in such systems (Figure 1).[3]

The process of internal conversion is a very fast process that can occur between excited states of the same multiplicity, for example, $^4T_{2g}$ and $^4T_{1g}$ states (Figure 1). Another process very common for O_h Cr (III) complexes is ISC that can occur between the states of different multiplicities, i.e., between quartet and doublet states. It is usually very efficient and for most of those systems results in the $^2E_g \rightarrow {}^4A_{2g}$ phosphorescence. In these systems, spin-orbit coupling is relatively weak[8] and non-radiative transitions, i.e., crossing of different spin PESs are driven by small energy gaps. The small energy
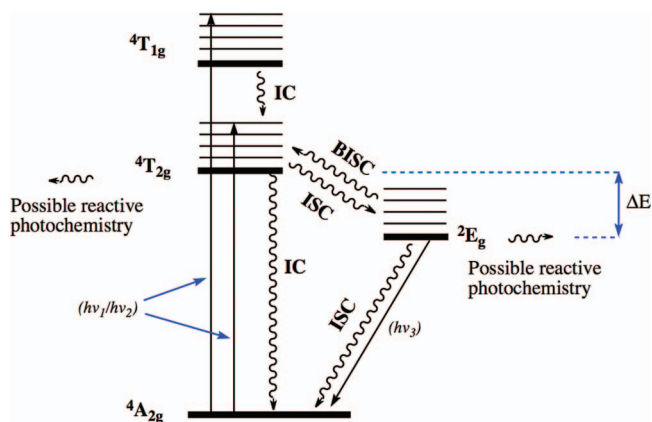

FIG. 1. Jablonski diagram for O_h Cr (III) complexes – full black lines with arrows represent absorption or emission processes, black wavy lines with arrows represent radiationless deactivation processes. Adapted from Ref. 3.

difference ΔE between $^4T_{2g}$ and ^2E_g states can also lead to a BISC process, which can induce $^4E_{2g} \rightarrow {}^4A_{2g}$ emission.[3,9]

B. Structural and spectroscopic properties of $[Cr(C_2O_4)_3]^{3-}$

$[Cr(C_2O_4)_3]^{3-}$ belongs to the family of complexes in which a Cr (III) ion is surrounded by six oxygen atoms (CrO_6). This is very common for oxide crystals such as ruby, emerald or alexandrite. In ruby Cr (III) ions exchange their position with Al atoms from sets of Al_2O_3 units, depending on the concentration of Cr (III). Ruby proved to be a very efficient fluorescent material at low temperatures due to the presence of Cr (III), and contains ~0.003%–1% of Cr_2O_3 units. In ruby oxygen atoms are coordinated to Cr (III) ions in nearly octahedral (O) positions with the site symmetry of Cr as C_3, and the point group symmetry as D_3, the same as in $[Cr(C_2O_4)_3]^{3-}$. Thus, the $[Cr(C_2O_4)_3]^{3-}$ system, as already mentioned is often called a "molecular version of ruby." The schematic picture of a single $Cr(C_2O_4)$ unit is presented in Figure 2 (calculated DFT structural parameters are given in Table I).

The excited state characteristics and kinetics of the excited state decay of Cr (III) complexes in oxygen
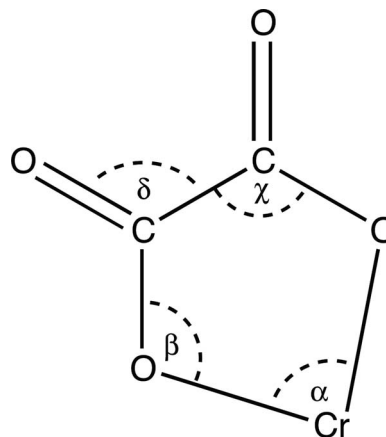

FIG. 2. Structure of single $Cr(C_2O_4)$ unit.

TABLE I. Main structural parameters of Cr (III) oxalato systems. DFT calculations performed using B3LYP functional. CASSCF calculations performed using SDD basis set for Cr atom and 6-31g(d,p) for O and C atoms.

Basis set	Bond lengths (Å)				Internal bond angles (Deg)			
	Cr–O	C–C	C=O	C–O	α	β	χ	δ
Calculated for $[Cr(C_2O_4)_3]^{3-}$								
aug-cc-pVTZ all atoms	2.01	1.58	1.23	1.29	80	117	113	121
aug-cc-pVTZ[a] all atoms	1.99	1.57	1.23	1.29	81	116	113.5	121
SDD – Cr; aug-cc-pVTZ – O, C	2.01	1.58	1.24	1.29	80	117	113	121
cc-pVTZ all atoms	2.01	1.57	1.23	1.29	80	117	113	121
SDD – Cr; 6-31g(d,p) – O, C	2.01	1.57	1.24	1.30	81	116	113	121
SDD – Cr[a]; 6-31g(d,p) – O, C	1.99	1.56	1.23	1.30	82	115	114	121
LANL2DZ all atoms	2.00	1.58	1.26	1.32	80	118	112	122
CAS1	2.01	1.56	1.21	1.27	79	117	113	120
CAS2	2.01	1.56	1.21	1.27	79	117	113	120
Calculated for $K_3[Cr(C_2O_4)_3]$								
LANL2DZ all atoms	1.99	1.58	1.27	1.30	82	116	113	120
cc-pVTZ – Cr, O, C; SDD – K[a]	2.00	1.56	1.23	1.29	82	115	114	120
Experimental data								
Experiment I (Refs. 28 and 29) $K_3[Cr(C_2O_4)_2(H_2O)_2] \cdot 3H_2O$	1.92		1.19	1.30		111		117
		1.39			83		125	
	1.93		1.28	1.32		112		118
Experiment II (Refs. 29 and 30) $K_3[Cr(C_2O_4)_3] \cdot 3H_2O$			1.25	1.47				
	1.88	1.23			81			
			1.17	1.42		…	…	…
	1.93	1.27			74			
			1.07	1.28				
Experiment III (Ref. 10) $(C_2O_4)^{2-}$	…	1.54	1.23	1.36	…	…	115	121

[a]PCM model with water as a solvent.

environments have been described, for example, based on crystal field theory, by Forster.[8] The ground state for these D_3 systems is an open-shell quartet with 3 electrons occupying a t_2 orbital $^4A_2(t_2{}^3)$ in the O representation. In most CrO_6 complexes, the excited $^4T_2$ state appears above the ^2E state (as shown in Figure 1), and the difference in energy ΔE between these states is quite small. The ΔE between these states and their ordering is especially important for the emission and thermal relaxation properties of a given CrO_6 systems, but it is very hard to determine the exact energies of ^2E and $^4T_2$ states.[8]

III. COMPUTATIONAL DETAILS

$[Cr(C_2O_4)_3]^{3-}$ has a pseudo-O_h (O) symmetry at the metal centre, however, as mentioned before, the symmetry of the full system is D_3. Computationally we use an Abelian point group symmetry, and for this system the largest Abelian subgroup of D_3 is C_2. In Table 1 in the supplementary material,[17] we detail the descent in symmetry of irreducible representations from the idealised O_h to actual D_3, to the used C_2 point group.

The states of Cr (III) systems are often discussed in terms of local O_h or O symmetry. In this paper, we use these labels for general discussion. For our report on $[Cr(C_2O_4)_3]^{3-}$, we use mainly the D_3 labels, however, T_1 and T_2 states (for O), which in D_3 symmetry are combinations of $(E+A_1)$ or $(E+A_2)$ states will be labelled as T states.

Density functional theory was used for determination of the ground state structure of the $[Cr(C_2O_4)_3]^{3-}$ complex. The B3LYP functional with a variety of different basis sets was used for structure optimizations. The symmetry of a system was kept as D_3. The effect of solvent was examined using a self-consistent polarizable continuum model (PCM) (Refs. 18 and 19) as implemented in the GAUSSIAN 09 program[20] with water as a solvent. Figure 3 presents both optical isomers of this system.

The infrared (IR) vibrational spectrum was calculated using the B3LYP functional, with water as a solvent (PCM model), and a cc-pVTZ basis set used on all atoms, imposing symmetry while calculating the vibrational frequencies. These results are compared with experiment and are presented in Table II. Given that $[Cr(C_2O_4)_3]^{3-}$ is an anionic compound the use of a basis set that includes diffuse functions may be of importance. However, our calculations show that the
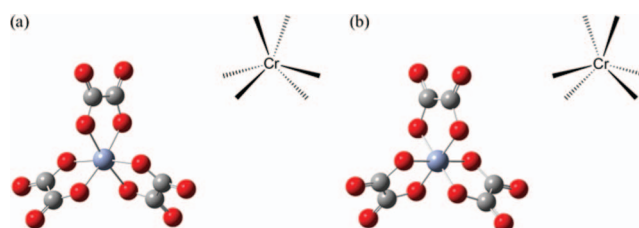

FIG. 3. Left (a) and right (b) (L-, R-) optical isomers of $[Cr(C_2O_4)_3]^{3-}$ system.

TABLE II. Comparison of calculated IR vibrations (B3LYP - PCM, with water as a solvent and cc-pVTZ basis set) in cm^{-1} to experiment.[29,31]

Calculated (PCM)	Symmetry[a]	Assignment	Experiment	Assignment
39	E	d_s C$_3$ axis	…	…
61	A$_1$	d_a C$_3$ axis	…	…
219, 222	E	v(M–O)+d(O–M–O)	…	…
286, 288	E	v(M–O)+ ring def.	…	…
…	…	…	313	out of plane (?)[b]
340, 347, 353	T	d(O–C = O)+v(C–C)	358	d(O–C = O)+v(C–C)
389, 400, 402	T	v$_a$(M–O)+ring def.	415	v(M-O)+ring def.
484, 486	T	ring def.+d(O–C = O)	485	ring def.+d(O–C = O)
524	E	v(M–O)+v(C–C)	543	v(M–O)+v(C–C)
…	…	…	595	crystal water(?)[c]
796, 805	E	d(O–C = O)+v(M–O)	798, 810	d(O–C = O)+v(M–O)
891	E	v(C–C)+d(O–C = O)	893	v$_s$(C–O)+d(O–C = O)
1264, 1266	T	v(C–O)+d(O–C = O)	1253	v$_s$(C–O)+d(O–C = O)
1367	E	d(O–C = O)+v(C–C)	1387	v$_s$(C–O)+v(C–C)
1691, 1694	T	v$_a$(C = O)+ring def.+d(O–C = O)	1684, 1660	v$_a$(C = O)
…	…	…	1708	v$_a$(C = O)

Note: d, d_s, d_a – deformation, symmetric/anti-symmetric deformation, v, v_s, v_a – vibration, symmetric/anti-symmetric vibration, ring def. – ring deformation.
[a]D$_3$ Symmetry of a full complex–T label represents a combination of either (E+A$_2$) or (E+A$_1$) excited states.
[b](?)–Uncertainty in the experimental assignment.
[c]Crystal water–description from Ref. 31 not further described.

optimized geometrical parameters obtained with DFT did not differ between the calculations using basis sets that do not include diffuse functions (such as cc-pVTZ) and a basis that does (such as aug-cc-pVTZ). These results and good agreement of the calculated IR vibrational data with experiment indicates that such bases are qualitatively suitable here. We further note that tests with highly diffuse sets had only a very minor contribution to the occupied Kohn-Sham orbitals. Thus, for CASSCF calculations as discussed below we did not use any diffuse functions to describe the d-electron states of the system. This represents a major computational saving as well as is helping to avoid convergence issues.

The electronic spectroscopy was studied using the TD-DFT method. TD-B3LYP and the Coulomb attenuated extension TD-CAM-B3LYP (Ref. 21) with the cc-pVTZ basis set for all atoms were used to study the UV-Vis spectroscopy of the system. We have examined the effect of diffuse basis sets on the calculated electronic spectra of the system for the lower lying states of interest and found the effects to be small: a 0.05–0.1 eV blueshift was observed for some metal d-d states depending on the functional used. These results are not discussed further below. To characterise important excited states of the system natural transition orbitals (NTOs) with TD-DFT were used.[22] These results are presented in Sec. IV.

CASSCF calculations in the gas phase were performed using the Stuttgart/Dresden (SDD) pseudo-potential on chromium and the 6-31g(d,p) basis set on oxygen and carbon. Two different active spaces were chosen for comparison. The first active space (CAS1) chosen consisted of 9 electrons and 11 orbitals based on approximate natural orbitals generated from a symmetry broken UHF calculation.[23] This strategy has been successfully utilised to study inorganic photochemistry previously,[14] and in particular in the study of the related [Cr(tn)$_3$]$^{3+}$ system.[16] The second active space (CAS2) consisted of 9 electrons and 11 orbitals with 1 orbital of p

character and 5 metal 3d orbitals and their 4d counterparts, which were generated using unrestricted B3LYP. This second strategy has been used in Refs. 24–27 with much success for inorganic complexes. Both guess sets of orbitals converged to the same CASSCF solution, giving confidence that the converged active space correctly describes the multiconfigurational character in this system. We note that further dynamic correlation can be added via, for example, CASPT2, but we have chosen not to in this study for the following two reasons, (i) we are using gradient driven methodologies to get a mechanistic understanding of the reactive photochemistry, and as such all the states of interest are d-electron states and at the current CASSCF level these are expected to be qualitatively well described, and even semi-quantitatively based on previous work,[24–27] (ii) a fragmented active space such as that described above appears to give rise to intruder states that complicate a CASPT2 approach. There are formalisms, such as RASSCF or NEVPT2, that could potentially be used to give superior energetics, but again we iterate that the scope of this paper is more illustrative and focuses on the crossing pathways that influence the reactive photochemistry of the system.

The CASSCF method uses spin-adapted configuration state functions (CSFs), which are linear combinations of Slater determinants (SD). Unlike the SDs, CSFs are eigenfunctions of $\hat{S}^2$, the total spin operator. Thus, CASSCF provides a good way of dealing with open-shell configurations of molecules. The (9,11) active space discussed above generates 76 230 quartet configurations. CI searches were performed in the quartet manifold as detailed below. These calculations were performed without constraining the geometrical symmetry to allow the system to break it if appropriate. ISC searches between quartet and doublet states were performed using the same optimisation algorithm as for CI searches. For these a many-electron basis of SDs of common M$_S$ value of +1/2 was used. Setting the multiplicity of a CASSCF

calculation to the lower doublet spin state (expectation value $\langle \hat{S}^2 \rangle$ of 0.75) allows the determination of states of the same and higher spin (in this case quartet spin states $\langle \hat{S}^2 \rangle$ of 3.75) in a SD many-electron basis.

All DFT, TD-DFT, and CASSCF calculations were performed using the GAUSSIAN 09 program.[20]

IV. RESULTS AND DISCUSSION

Calculated geometrical parameters of the complex have been compared to experimental values and are presented in Table I. Calculated solvent effects are small and only a slight shortening (0.01–0.02 Å) of Cr–O and C–C bonds was observed for calculations using a solvent model.

There are slight differences between calculated geometrical parameters of $[Cr(C_2O_4)_3]^{3-}$ and experimental ones depending on which experimental results we compare them to. Computations with different DFT functionals and basis sets for the full complex, as specified in Table I, give very good agreement to experimental parameters for the free $(C_2O_4)^{2-}$ ligand (Experiment III; Ref. [10]). However, there is an elongation of C–C bonds of 0.16 Å to even 0.33 Å comparing our calculations with available experimental data for the full complex.[28–30] It should be noted that the experimental parameters were obtained from different crystalographic data where the $[Cr(C_2O_4)_3]^{3-}$ system is incorporated into neutral coordination networks (for example, $K_3[Cr(C_2O_4)_3] \cdot 3H_2O$).[29,30] The standard C–C single bond for a single oxalate ion $(C_2O_4)^{2-}$ obtained from a x-ray diffraction experiment is around 1.54 Å.[10] However, experimental studies on the full complex show shorter C–C single bonds. Our calculations on the full $[Cr(C_2O_4)_3]^{3-}$ complex show the same C–C bond length as for the single $(C_2O_4)^{2-}$ ion. The shorter C–C bond obtained in the experimental data of the full complex[30] could be due to some contraction or packing forces in the solid state. DFT calculations on a model $K_3[Cr(C_2O_4)_3]$ system were also performed and this did not have any major effects on geometrical parameters.

Infrared spectroscopy is very important in the structural determination of such systems. We have computed and assigned the IR vibrational spectrum of $[Cr(C_2O_4)_3]^{3-}$ using DFT. These were calculated using the B3LYP functional with water as a solvent (Table II). Despite some possible discrepancies in the calculated and experimental structural parameters of $[Cr(C_2O_4)_3]^{3-}$, a good agreement of experimental and calculated IR is observed. There were some uncertainties in the character of vibrations located at 313 cm^{-1} and 595 cm^{-1}, however, none of these were reproduced in our calculations. To our knowledge this is the first attempt to assign the IR spectrum in a complex such as this, and very reasonable agreement can be seen between experiment and theory for this open-shell complex. We note that for most vibrations DFT assignment complements experimental assignment very well.

It is known that $[Cr(C_2O_4)_3]^{3-}$ is stable with respect to exposure to visible light, i.e., this has no influence on the absorption spectra. It was experimentally found that the main absorption bands are broad spin-allowed d-d transitions at 570 nm and 420 nm attributed to $^4T_2 \leftarrow {}^4A_2$ and $^4T_1 \leftarrow {}^4A_2$, respectively, and two bands at 270 nm and 224 nm attributed to ligand to metal charge transfer.[31] The main emissive feature is a sharp band at 697 nm attributed to a spin-forbidden $^2E \rightarrow {}^4A_2$ transition. Table III presents the UV-Vis spectral features of the $[Cr(C_2O_4)_3]^{3-}$ complex calculated using the CAM-B3LYP functional and how they are influenced by the presence of solvent using a PCM.

The calculated positions of the spectral bands using TD-DFT are with reasonable agreement with experiment. The band located experimentally at 570 nm shows a blueshift for the calculated spectra of 0.26–0.41 eV. There is only little influence of the aqueous solvent on this band of 0.15 eV (blueshift comparing to calculation in the gas phase). The band located at 697 nm, assigned to $^2E \rightarrow {}^4A_2$ emission, is not reproduced with the standard TD-DFT method used here, although we note that spin-flip approaches to TD-DFT have recently been developed (spin adapted TD-DFT) that deal with open-shell systems and include both spin-conserving and spin-flip excitations. However, these methods are in their infancy and have not seen general use as of yet.[32,33] The assignment of the transitions located between 200 nm and 300 nm is not straightforward due to the large number of states involved. These states do not have any dominant configuration that would describe the nature of excitation. The NTO method creates a compact orbital representation of the electronic transition density matrix. Unitary transformations are applied separately to occupied and virtual orbitals and from this the best possible representation between the excited electronic density and hole created after excitation is established.[22] Using NTOs it was determined that the nature of the bands between 200 nm and 300 nm are very mixed with some ligand to metal and metal to ligand CT character. Both the 400 nm and 500 nm bands have

TABLE III. Main absorption spectral bands of $[Cr(C_2O_4)_3]^{3-}$ (in nm (eV)) with oscillator strengths f and their symmetries using D_3 irreducible representations[a]: TD-DFT using the cc-pVTZ basis set on all the atoms; and previous experimental findings.[31]

Symmetry	TD-B3LYP Gas phase	f	TD-B3LYP In solvent	f	TD-CAM-B3LYP Gas phase	f	TD-CAM-B3LYP In solvent	f	Experiment
T	240 (5.17)	0.0072	240 (5.17)	0.0036	200 (6.20)	0.0131	200 (6.20)	0.0231	224 (5.53)
E	270 (4.59)	0.0036	270 (4.59)	0.0073	250 (4.96)	0.0018	250 (4.96)	0.0031	270 (4.59)
E	410 (3.03)	0.0012	400 (3.10)	0.0012	400 (3.10)	0.0010	390 (3.18)	0.0011	420 (2.95)
T	520 (2.38)	0.0003	500 (2.48)	0.0003	510 (2.43)	0.0002	480 (2.58)	0.0003	570 (2.17)
									697 (1.78)

[a]T symmetry label is used for the combination of states (E+A$_2$) or (E+A$_1$) in D_3 irreducible representations of the complex; oscillator strengths given in this table come from the E component of the T state.

TABLE IV. Ordering of electronically excited states in $[Cr(C_2O_4)_3]^{3-}$ (CASSCF: SDD for Cr and 6-31g(d,p) basis set for C and O atoms). Vertical energies taken from a CASSCF calculation (using a Slater determinant (SD) many-electron $M_S = +1/2$ basis) with orbitals state averaged over 12 states.

State	Configuration	Energy (eV)
Ground state	$^4A_2$ (t_2^3)	0
1	^2T (t_2^3)	2.08
2	^2E (t_2^3)	2.51
3	^2T (t_2^3)	2.64
4	^2E $(t_2^2 e)$	3.12
5	^4T $(t_2^2 e)$	3.34

FIG. 4. General picture of potential energy surfaces (PES) for ground and non-adiabatically coupled excited states of the $[Cr(C_2O_4)_3]^{3-}$ complex (dc–derivative coupling vector, gd–gradient difference vector, ISC–intersystem crossing, CI–conical intersection, TBP–trigonal bipyramid).

d-d character and are in agreement with previous experimental conjecture.[10,31] It should be noted that there is also a large degree of spin contamination for some excited states using TD-DFT especially for the higher lying states (for example, states located between 270–280 nm and 4.42–4.59 eV instead of having $\langle S^2 \rangle$ equal to 3.75 for quartet states, have $\langle S^2 \rangle$ of around 5). CASSCF in contrast is a pure spin method. Table IV presents the ordering of CASSCF excited states, their dominant electronic configurations, and vertical energies. Ordering of these states must be treated in caution due to the lack of extra dynamical correlation in the CASSCF method and they are shown here for a qualitative picture only.

Note that for multiply degenerate T and E states there is one electronic state per component of the degenerate group, e.g., 3 CASSCF roots for one T state. The energy of the first quartet-excited state (^4T) using this state averaged wavefunction is equal to 3.34 eV, which is around 0.75–1.2 eV away from experiment and TD-DFT. It should be noted here that this difference may be due to the quite large state-averaging used. For the state specific calculations of the ^4T state, starting from the quartet manifold of the system (using many electron CSFs rather than SDs), the energy of the ^4T state is equal to 2.05 eV which is in much better agreement with TD-DFT computed excitations and experimental data.

To determine possible crossings of PESs in this system, CI searches using CASSCF between the ground $^4A_2$ state and first quartet excited state (^4T) were performed starting from the R-optical isomer. It should be noted here that the T state here is a combination of E and A_2 states in the D_3 representation, however, the labelling will remain unchanged, and the first quartet excited state will be considered as ^4T state. In our calculations away from the ground state minimum, the D_3 symmetry was further broken and we only consider one component of this T state. A peaked CI connecting both ^4T and $^4A_2$ states has been found (Figure 4), allowing for efficient transition from the excited state to the ground state PES. Figure 4 presents a general picture of PES crossings in this system.

The structure of $[Cr(C_2O_4)_3]^{3-}$ at this optimised CI point can be characterised by an elongation and rupture of a single Cr–O bond (Figure 5), to generate a quasi-trigonal bipyramid (quasi-TBP) structure.
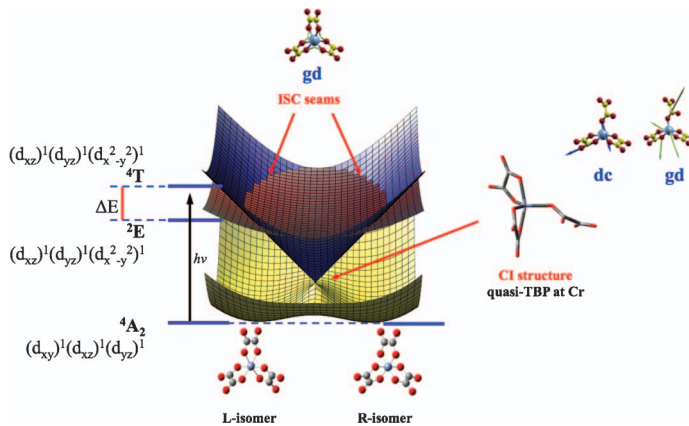
Similar behaviour, i.e., dissociation of single Cr–O bond was noted for the oxygen exchange process between $[Cr(C_2O_4)_3]^{3-}$ system and a solvent water, which can be thought of as a parallel to the racemization.[10] In the experimental studies, it was assumed that the rupture of a Cr–O bond is a result of photoactivation of $[Cr(C_2O_4)_3]^{3-}$ complex.[10] The above computational findings prove that indeed it is the case. The coordination at the metal centre of the $[Cr(C_2O_4)_3]^{3-}$ system, at the point of CI, is quasi-TBP (Figure 4). This structure is similar to a Jahn-Teller active structure that will efficiently distort to form a minimum on the ground state PES. The ruptured end of C_2O_4 ligand can clip back on, via motion in the branching space of this CI (shown in Figure 4) to form either the R-isomer or L-isomer of the complex. This mechanism explains the racemization of this system, which as mentioned above was experimentally found to be photoinduced.[10,12] This is supported by the fact that the character of CI involved in this reaction is peaked which could lead to more than one photoproduct on the ground state PES, i.e., the original stereoisomer or its alternative form (Figure 4).

The presence of this CI between the ^4T state of $(d_{xz})^1(d_{yz})^1(d_{x^2-y^2})^1$ configuration and $^4A_2$ state of $(d_{xz})^1(d_{yz})^1(d_{xy})^1$ configuration can be explained by the fact that at the TBP geometries at the metal centre (found at the optimised point of CI) the $d_{x^2-y^2}$ and d_{xy} orbitals become degenerate. Figure 6 presents the orbital configurations of
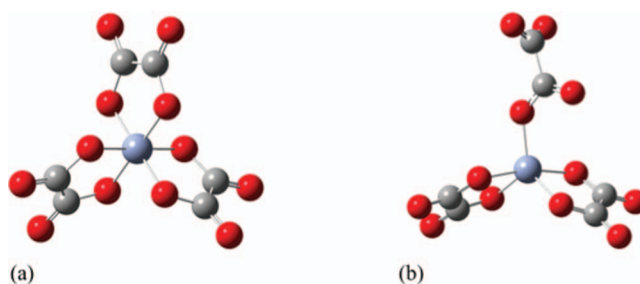

FIG. 5. The structure of the $[Cr(C_2O_4)_3]^{3-}$ complex (R-isomer) (a) at the ground state, (b) at the minimum energy CI point.
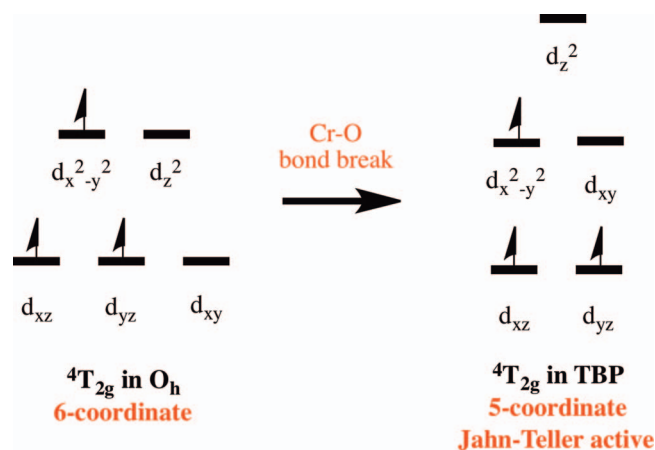
FIG. 6. Change in orbital configuration when distorting from O_h symmetry of given metal centre ($^4T_{2g}$ state) to D_3 symmetry ($^4(A_1 \oplus E)$ state) in $[Cr(C_2O_4)_3]^{3-}$.

the $^4T_{2g}$ state when the molecule is distorted from O_h to TBP via breakage of a single coordination site. Distortion from this point removes the degeneracy in these orbitals and the system can easily move onto the ground state PES with a $(d_{xz})^1(d_{yz})^1(d_{xy})^1$ configuration. Thus, the absorption of a photon can rupture a single Cr–O bond allowing the now 5-coordinate system to adopt a quasi-Jahn-Teller geometry that connects the excited and ground quartet states. This has similarities to photodissociation of binary transition metal carbonyls, in which after photoinduced loss of a single CO ligand, the unsaturated complex relaxes to the ground electronic state on an ultrafast timescale through a Jahn-Teller degeneracy imposed CI.[15,27]

This reaction can also be quenched by the presence of a close lying ^2E state of the same configuration as ^4T state. Studies on the presence of ISC between those states were performed and the results are presented below.

CASSCF calculations, as described in Sec. III, have been performed to determine the presence of $^4T \rightarrow \, ^2E$ ISC seams. The 3N-7 dimensional intersection seams between the PESs of a quartet and doublet excited state have been located (note that the derivative coupling vector on this seam is zero due to symmetry, and thus there is only a non-zero gradient difference vector present), which did not involve any dramatic change in geometrical parameters confirming experimental reasoning (Figure 4), i.e., the minimum energy points on the seam correspond to reasonably well-defined R- or L-optical isomers. The ISC seams have a locally sloped topology (as depicted in Figure 4). This ISC seam is equivalent for both R- and L-isomers of $[Cr(C_2O_4)_3]^{3-}$. The presence of these ISC seam minima is not so surprising as the electronic configuration of the ^4T state is the same as the electronic configuration of the ^2E state, namely, $(d_{xz})^1(d_{yz})^1(d_{x^2-y^2})^1$. Crossing from one state to another would not require any change in orbital occupation but only flipping of the spin. For 1st row transition metal valence electrons, the spin-orbit coupling is expected to be relatively weak. Indeed, experimental studies on the optical absorption spectrum of $[Cr(C_2O_4)_3]^{3-}$ system doped in $NaMg[Al(C_2O_4)_3]8H_2O$ show a splitting of about 2–3 cm^{-1} of doublet bands arising from $^2E_g(O_h)$ in the α- and

π spectrum.[34] Thus, the driving force for the ISC occurring is the small ΔE energy difference between the states, having maximum efficiency at geometries where the pure spin-state PESs cross.

V. CONCLUSIONS

To conclude we have presented studies on the photochemistry and excited state relaxation pathways through quartet and doublet manifolds of the $[Cr(C_2O_4)_3]^{3-}$ system that is important due to its energy migration features which are similar to those in ruby. These processes have not been theoretically studied in any detail due to the complexity of Cr (III) systems. The IR and UV-Vis spectroscopy have been examined using DFT and its TD extension, respectively. The calculated IR spectra is in good agreement with the experimental one, showing that the DFT method can be a very useful, cost efficient alternative, for the examination of ground state properties of large open-shell transition metal complexes. The performance of the TD-DFT method for the UV-Vis spectroscopy of open-shell transition metal systems can often be worse than that for closed-shell systems due to significant spin contamination. Here, the main features of the electronic spectra are reasonably well reproduced although the higher energy bands show a large degree of state mixing. Mechanisms for radiationless deactivation through the quartet and doublet manifolds were examined using the multiconfigurational CASSCF method. A conical intersection seam between the $^4A_2$ ground state and one component of the ^4T excited state was located, involving a rupture of one of the Cr–O bonds and its rearrangement to an unsaturated intermediate. The coordination of the metal centre at the CI minimum becomes TBP, which is quasi-Jahn-Teller and from there the system distorts to either stereoisomeric minima on the ground PES. Due to the peaked character of this CI, both the R- and L- forms are realised, accounting for the photoinduced racemization. ISC seams between the ^2E and ^4T states have been located that did not involve any major change in geometrical parameters of the system. This is a possible pathway that ultimately leads to the $^2E \rightarrow \, ^4A_2$ emission seen experimentally.

[1]L. S. Forster, Chem. Rev. **90**, 331 (1990).
[2]D. K. Geiger, Coord. Chem. Rev. **152**, 359 (1996).
[3]N. A. P. Kane-Maguire, Top. Curr. Chem. **280**, 37 (2007).
[4]A. D. Kirk, Comments Inorg. Chem. **14**, 89 (1993).
[5]A. D. Kirk, Chem. Rev. **99**, 1607 (1999).
[6]A. D. Kirk and G. Irwin, Coord. Chem. Rev. **211**, 25 (2001).
[7]M. Milos, S. Kairouani, S. Rabaste, and A. Hauser, Coord. Chem. Rev. **252**, 2540 (2008).
[8]L. S. Forster, Coord. Chem. Rev. **248**, 261 (2003).
[9]L. S. Forster, Coord. Chem. Rev. **227**, 59 (2002).
[10]K. V. Krishnamurty and G. M. Harris, Chem. Rev. **61**, 213 (1961).

[11] A. W. Adamson and S. T. Spees, in *Proceedings of the International Conference on Coordination Chemistry, London*, 1959.

[12] S. T. Spees and A. W. Adamson, Inorg. Chem. **1**, 531 (1962).

[13] J. M. Żurek and M. J. Paterson, Inorg. Chem. **48**, 10652 (2009).

[14] J. M. Żurek and M. J. Paterson, J. Phys. Chem. Lett. **1**, 1301 (2010).

[15] R. G. McKinlay, J. M. Żurek, and M. J. Paterson, Adv. Inorg. Chem. **62**, 351 (2010).

[16] J. M. Żurek and M. J. Paterson, J. Phys. Chem. A **116**, 5375 (2012).

[17] See supplementary material at http://dx.doi.org/10.1063/1.4736561 for descent in symmetry from O_h to C_2 point groups.

[18] G. Scalmani, M. J. Frisch, B. Mennucci, J. Tomasi, R. Cammi, and V. Barone, J. Chem. Phys. **124**, 94107 (2006).

[19] G. Scalmani and M. J. Frisch, J. Chem. Phys. **132**, 114110 (2010).

[20] M. J. Frisch, G. W. Trucks, H. B. Schlegel, G. E. Scuseria, M. A. Robb, J. R. Cheeseman, G. Scalmani, V. Barone, B. Mennucci, G. A. Petersson, H. Nakatsuji, M. Caricato, X. Li, H. P. Hratchian, A. F. Izmaylov, J. Bloino, G. Zheng, J. L. Sonnenberg, M. Hada, M. Ehara, K. Toyota, R. Fukuda, J. Hasegawa, M. Ishida, T. Nakajima, Y. Honda, O. Kitao, H. Nakai, T. Vreven, J. A. Montgomery, Jr., J. E. Peralta, F. Ogliaro, M. Bearpark, J. J. Heyd, E. Brothers, K. N. Kudin, V. N. Staroverov, R. Kobayashi, J. Normand, K. Raghavachari, A. Rendell, J. C. Burant, S. S. Iyengar, J. Tomasi, M. Cossi, N. Rega, J. M. Millam, M. Klene, J. E. Knox, J. B. Cross, V. Bakken, C. Adamo, J. Jaramillo, R. Gomperts, R. E. Stratmann, O. Yazyev, A. J. Austin, R. Cammi, C. Pomelli, J. W. Ochterski, R. L. Martin, K. Morokuma, V. G. Zakrzewski, G. A. Voth, P. Salvador, J. J. Dannenberg, S. Dapprich, A. D. Daniels, Ö. Farkas, J. B. Foresman, J. V. Ortiz, J. Cioslowski, and D. J. Fox, GAUSSIAN 09, Revision A.2, Gaussian, Inc., Wallingford CT, 2009.

[21] B. J. Persson, B. O. Roos, and K. Pierloot, J. Chem. Phys. **101**, 6810 (1994).

[22] R. L. Martin, J. Chem. Phys. **118**, 4775 (2003).

[23] P. Pulay and T. P. Hamilton, J. Chem. Phys. **88**, 4926 (1988).

[24] G. A. Worth, G. Welch, and M. J. Paterson, Mol. Phys. **104**, 1095 (2006).

[25] M. J. Paterson, P. A. Hunt, M. A. Robb, and O. Takahashi, J. Phys. Chem. A **106**, 10494 (2002).

[26] M. J. Paterson, L. Blancafort, S. Wilsey, and M. A. Robb, J. Phys. Chem. A **106**, 11431 (2002).

[27] R. G. McKinlay and M. J. Paterson, in *The Jahn-Teller Effect: Advances and Perspectives; Springer Series in Chemical Physics*, edited by H. Köppel, H. Barentzen, and D. R. Yarkony (Springer, Heidelberg, 2010), p. 311.

[28] J. N. van Niekerk and F. R. L. Schoening, Acta Cryst. **4**, 35 (1951).

[29] J. Fujita, A. E. Martell, and K. Nakamoto, J. Chem. Phys. **36**, 324 (1962).

[30] J. N. van Niekerk and F. R. L. Schoening, Acta Cryst. **4**, 381 (1951).

[31] R. A. Condrate and L. S. Forster, J. Mol. Spectrosc. **24**, 490 (1967).

[32] Z. D. Li and W. J. Liu, J. Chem. Phys. **133**, 064106 (2010).

[33] Z. D. Li, W. J. Liu, Y. Zhang, and B. B. Suo, J. Chem. Phys. **134**, 134101 (2011).

[34] T. Schönherr, J. Spanier, and H. H. Schmidtke, J. Phys. Chem. **93**, 5969 (1989).